Electronic Supplementary Material (ESI) for Physical Chemistry Chemical Physics.

Supporting Information

Towards Developing Efficient Metalloporphyrin-Based Hybrid Photocatalysts for CO_2 Reduction; An Ab Initio Study

Azar Ostovan,[†] Nick R. Papior,[‡] Mansour Zahedi,[¶] and Alireza Z. Moshfegh[*,†,§]

[†]*Department of Physics, Sharif University of Technology, Tehran 11155-9161, Iran*

[‡]*DTU Computing Center, Department of Applied Mathematics and Computer Science, Technical University of Denmark, DK-2800 Kongens Lyngby, Denmark*

[¶]*Faculty of Chemical and Petroleum Sciences, Shahid Beheshti University G.C., P.O. Box 19839-63113, Evin, Tehran 19839, Iran*

[§]*Institute for Nanoscience and Nanotechnology, Sharif University of Technology, Tehran 14588-8969, Iran*

E-mail: moshfegh@sharif.edu

Phone: +98 (0)21 6616 4516. Fax: +98 (0)21 6602 2711

Table S1. Functional optimization for the CoPor complex. Comparison is carried out between previous experimental bond lengths (d) and the calculated ones. All structures were relaxed with LANL2DZ for metal-ion and the 6-31+G(d,p) basis set for the rest of atoms. The C_α and C_β positions are shown in Figure S1a.

Functional	d(Co−N)/Å	d(N−C_α)/Å	d(C_α−C_β)/Å	d(C_β−C_β)/Å	RMSE/Å
B3LYP	1.98	1.39	1.45	1.37	0.013
OPBE	1.98	1.40	1.45	1.37	0.017
PBEPBE	1.99	1.41	1.45	1.38	0.025
CAM-B3LYP	1.98	1.40	1.45	1.37	0.017
M06	1.98	1.39	1.44	1.37	0.012
ωB97XD	1.99	1.39	1.45	1.37	0.017
Experimental[1]	1.97	1.37	1.44	1.36	–

Table S2. Functional optimization for the NiPor complex. Comparison is carried out between previous experimental bond lengths (d) and the calculated ones. All structures were relaxed with LANL2DZ for metal-ion and the 6-31+G(d,p) basis set for the rest of atoms. The C_α and C_β positions are shown in Figure S1b.

Functional	d(Ni−N)/Å	d(N−C_α)/Å	d(C_α−C_β)/Å	d(C_β−C_β)/Å	RMSE/Å
B3LYP	1.98	1.40	1.45	1.37	0.021
OPBE	1.98	1.40	1.45	1.37	0.021
PBEPBE	1.98	1.41	1.45	1.40	0.021
CAM-B3LYP	1.97	1.40	1.45	1.37	0.021
M06	1.96	1.39	1.44	1.37	0.012
Experimental[2]	1.95	1.38	1.44	1.35	–

Table S3. Functional optimization for the CuPor complex. Comparison is carried out between previous experimental bond lengths (d) and the calculated ones. All structures were relaxed with LANL2DZ for metal-ion and the 6-31+G(d,p) basis set for the rest of atoms. The C_α and C_β positions are shown in Figure S1c.

Functional	d(Cu−N)/Å	d(N−C_α)/Å	d(C_α−C_β)/Å	d(C_β−C_β)/Å	RMSE/Å
B3LYP	2.03	1.39	1.45	1.37	0.025
OPBE	2.04	1.39	1.45	1.38	0.032
PBEPBE	2.04	1.40	1.46	1.38	0.032
CAM-B3LYP	2.02	1.38	1.45	1.37	0.022
M06	2.01	1.39	1.44	1.37	0.017
ωB97XD	2.09	1.37	1.46	1.37	0.045
Experimental[3]	1.98	1.39	1.45	1.36	–

Table S4. Functional optimization for the ZnPor complex. Comparison is carried out between previous experimental bond lengths (d) and the calculated ones. All structures were relaxed with LANL2DZ for metal-ion and the 6-31+G(d,p) basis set for the rest of atoms. The C_α and C_β positions are shown in Figure S1d.

Functional	d(Zn−N)/Å	d(N−C_α)/Å	d(C_α−C_β)/Å	d(C_β−C_β)/Å	RMSE/Å
B3LYP	2.04	1.38	1.45	1.37	0.007
OPBE	2.05	1.39	1.45	1.37	0.011
PBEPBE	2.05	1.39	1.45	1.38	0.012
CAM-B3LYP	2.03	1.38	1.45	1.36	0.009
M06	2.03	1.38	1.44	1.37	0.009
ωB97XD	2.04	1.38	1.45	1.36	0.009
Experimental[4]	2.04	1.37	1.45	1.37	–

Table S5. Comparison between required time for geometry optimization of isolated parts and its constructed hybrid photocatalyst using both B3LYP and M06 functionals. The calculation times (t, h:min) are obtained using the same 16-core node for all structure relaxations.

Functional	t(ED)/h:min	t(ZnPor)/h:min	t(ZnPor(ED)$_4$)/h:min
B3LYP	1:07	2:11	12:03
M06	2:01	3:39	30:18

Table S6. Basis set optimization for the CoPor. Comparison is carried out between previous experimental bond lengths (d) and the calculated ones. All structures were relaxed using B3LYP functional. The C_α and C_β positions are shown in Figure S1a.

Basis set	d(Co−N)/Å	d(N−C_α)/Å	d(C_α−C_β)/Å	d(C_β−C_β)/Å	RMSE/Å
LANL2DZ/6-31+G(d,p)	1.98	1.39	1.45	1.37	0.013
LACV3P/6-31++G(d,p)	1.97	1.39	1.44	1.36	0.010
Experimental[1]	1.97	1.37	1.44	1.36	–

Table S7. Basis set optimization for the NiPor. Comparison is carried out between previous experimental bond lengths (d) and the calculated ones. All structures were relaxed using B3LYP functional. The C_α and C_β positions are shown in Figure S1b.

Basis set	d(Ni−N)/Å	d(N−C_α)/Å	d(C_α−C_β)/Å	d(C_β−C_β)/Å	RMSE/Å
LANL2DZ/6-31+G(d,p)	1.98	1.40	1.45	1.37	0.021
LACV3P/6-31++G(d,p)	1.97	1.39	1.44	1.36	0.012
Experimental[2]	1.95	1.38	1.44	1.35	–

Table S8. Basis set optimization for the CuPor. Comparison is carried out between previous experimental bond lengths (d) and the calculated ones. All structures were relaxed using B3LYP functional. The C_α and C_β positions are shown in Figure S1c.

Basis set	d(Cu−N)/Å	d(N−C_α)/Å	d(C_α−C_β)/Å	d(C_β−C_β)/Å	RMSE/Å
LANL2DZ/6-31+G(d,p)	2.03	1.39	1.45	1.37	0.025
LACV3P/6-31++G(d,p)	2.02	1.39	1.45	1.37	0.021
Experimental[3]	1.98	1.39	1.45	1.36	–

Table S9. Basis set optimization for the ZnPor. Comparison is carried out between previous experimental bond lengths (d) and the calculated ones. All structures were relaxed using B3LYP functional. The C_α and C_β positions are shown in Figure S1d.

Basis set	d(Zn−N)/Å	d(N−C_α)/Å	d(C_α−C_β)/Å	d(C_β−C_β)/Å	RMSE/Å
LANL2DZ/6-31+G(d,p)	2.04	1.38	1.45	1.37	0.007
LACV3P/6-31++G(d,p)	2.05	1.39	1.45	1.37	0.01
Experimental[4]	2.04	1.37	1.45	1.37	–

Table S10. Calculated maximum wavelength (λ_{max}, nm) of the CoPor using different functionals.

Functional	CAM-B3LYP	LC-ωPBE	ωB97XD	BHandHLYP
	344.40	335.34	321.11	322.50
Theoretical[5]	492			

Table S11. Calculated maximum wavelength (λ_{max}, nm) of the NiPor using different long-range corrected functionals.

Functional	CAM-B3LYP	LC-ωPBE	ωB97XD	BHandHLYP
	349.69	348.42	348.15	323.33
Theoretical[5]	354			

Table S12. Calculated maximum wavelength (λ_{max}, nm) of the CuPor using different long-range corrected functionals.

Functional	CAM-B3LYP	LC-ωPBE	ωB97XD	BHandHLYP
	353.22	349.32	350.31	322.35
Experimental[6]	421			

Table S13. Calculated maximum wavelength (λ_{max}, nm) of the ZnPor using different long-range corrected functionals.

Functional	CAM-B3LYP	LC-ωPBE	ωB97XD	BHandHLYP
	360.86	351.48	360.80	327.73
Experimental[6]	429			

Table S14. Calculated optical properties of ED using different long-range corrected functionals in comparison with previous experimental work.

Functional	E_{HOMO} (eV)	E_{LUMO} (eV)	E_g (eV)	E_{opt} (eV)	λ_{max} (nm)
CAM-B3LYP	–	–	–	2.65	290.13, 467.75
LC-ωPBE	–	–	–	2.99	260.52, 414.03
ωB97XD	–	–	–	2.71	284.6, 456.65
Experimental[7]	-3.4	-5.8	2.4	2.44	310, 445

Table S15. Calculated maximum wavelength (λ_{max}) of the ZnPor(ED)$_n$ with $n = 1 - 4$.

Photocatalyst	λ_{max} (nm)
ZnPorED$_1$	375.76
ZnPorED$_2$	394.41
ZnPorED$_3$	492.42
ZnPorED$_4$	500.12

Table S16. The calculated relative stability energies (kcal mol^{-1}) of photocatalyst active site (MPor with M=Co, Ni, Cu and Zn) at their first three spin-states.

Photocatalyst active site	Singlet	Doublet	Triplet	Quartet	Quintet	Sexted
CoPor	–	0.00	–	6.90	–	17.72
NiPor	0.00	–	4.98	–	20.01	–
CuPor	–	0.00	–	13.76	–	28.33
ZnPor	0.00	–	14.67	–	31.36	–

Table S17. The calculated HOMO and LUMO energy levels and associated bandgaps (E_g, eV) for MPor(ED)$_4$ photocatalysts with M=Co, Ni, Cu and Zn.

Photocatalysts	E_{HOMO} (eV)	E_{LUMO} (eV)	E_g (eV)
CoPor(ED)$_4$	−4.74	−3.00	1.74
NiPor(ED)$_4$	−4.69	−2.98	1.71
CuPor(ED)$_4$	−4.65	−2.99	1.66
ZnPor(ED)$_4$	−4.62	−2.99	1.63

Table S18. The calculated HOMO and LUMO energy levels and associated bandgaps (E_g) for base MPors with M=Co, Ni, Cu and Zn.

MPor	E_{HOMO} (eV)	E_{LUMO} (eV)	E_g (eV)
CoPor	−5.26	−2.08	3.18
NiPor	−5.28	−2.12	3.16
CuPor	−5.22	−2.16	3.06
ZnPor	−5.14	−2.16	2.98

Table S19. The evaluated nature of transition associated with λ_{max} of CoPor(ED)$_4$.

CoPor(ED)$_4$	configuration coefficient
HOMO$-5(\alpha)\rightarrow$ LUMO$+1(\alpha)$	-0.15274
HOMO$-4(\alpha)\rightarrow$ LUMO(α)	0.22471
HOMO$-4(\alpha)\rightarrow$ LUMO$+5(\alpha)$	0.10192
HOMO$-3(\alpha)\rightarrow$ LUMO$+2(\alpha)$	0.23511
HOMO$-2(\alpha)\rightarrow$ LUMO$+3(\alpha)$	0.22507
HOMO$-1(\alpha)\rightarrow$ LUMO(α)	0.29469
HOMO$-1(\alpha)\rightarrow$ LUMO$+5(\alpha)$	-0.18096
HOMO$(\alpha)\rightarrow$ LUMO$+1(\alpha)$	-0.21965
HOMO$(\alpha)\rightarrow$ LUMO$+4(\alpha)$	-0.31891
HOMO$(\alpha)\rightarrow$ LUMO$+5(\alpha)$	0.12859
HOMO$-5(\beta)\rightarrow$ LUMO(β)	-0.13876
HOMO$-4(\beta)\rightarrow$ LUMO$+1(\beta)$	-0.21424
HOMO$-4(\beta)\rightarrow$ LUMO$+5(\beta)$	-0.11463
HOMO$-3(\beta)\rightarrow$ LUMO$+2(\beta)$	-0.22767
HOMO$-2(\beta)\rightarrow$ LUMO$+3(\beta)$	0.22683
HOMO$-1(\beta)\rightarrow$ LUMO$+1(\beta)$	-0.28602
HOMO$-1(\beta)\rightarrow$ LUMO$+5(\beta)$	0.20212
HOMO$(\beta)\rightarrow$ LUMO(β)	-0.18239
HOMO$(\beta)\rightarrow$ LUMO$+4(\beta)$	0.32426

Table S20. The evaluated nature of transition associated with λ_{max} of NiPor(ED)$_4$.

NiPor(ED)$_4$	configuration coefficient
HOMO$-5(\alpha)\rightarrow$ LUMO$+1(\alpha)$	-0.15274
HOMO$-4(\alpha)\rightarrow$ LUMO(α)	0.22471
HOMO$-4(\alpha)\rightarrow$ LUMO$+5(\alpha)$	0.10192
HOMO$-3(\alpha)\rightarrow$ LUMO$+2(\alpha)$	0.23511
HOMO$-2(\alpha)\rightarrow$ LUMO$+3(\alpha)$	0.22507
HOMO$-1(\alpha)\rightarrow$ LUMO(α)	0.29469
HOMO$-1(\alpha)\rightarrow$ LUMO$+5(\alpha)$	-0.18096
HOMO$(\alpha)\rightarrow$ LUMO$+1(\alpha)$	-0.21965
HOMO$(\alpha)\rightarrow$ LUMO$+4(\alpha)$	-0.31891
HOMO$(\alpha)\rightarrow$ LUMO$+5(\alpha)$	0.12859
HOMO$-5(\beta)\rightarrow$ LUMO(β)	-0.13876
HOMO$-4(\beta)\rightarrow$ LUMO$+1(\beta)$	-0.21424
HOMO$-4(\beta)\rightarrow$ LUMO$+5(\beta)$	-0.11463
HOMO$-3(\beta)\rightarrow$ LUMO$+2(\beta)$	-0.22767
HOMO$-2(\beta)\rightarrow$ LUMO$+3(\beta)$	0.22683
HOMO$-1(\beta)\rightarrow$ LUMO$+1(\beta)$	-0.28602
HOMO$-1(\beta)\rightarrow$ LUMO$+5(\beta)$	0.20212
HOMO$(\beta)\rightarrow$ LUMO(β)	-0.18239
HOMO$(\beta)\rightarrow$ LUMO$+4(\beta)$	0.32426

Table S21. The evaluated nature of transition associated with λ_{max} of CuPor(ED)$_4$.

CuPor(ED)$_4$	configuration coefficient
HOMO$-5(\alpha) \rightarrow$ LUMO(α)	-0.14828
HOMO$-4(\alpha) \rightarrow$ LUMO(α)	0.23296
HOMO$-4(\alpha) \rightarrow$ LUMO$+5(\alpha)$	-0.10424
HOMO$-2(\alpha) \rightarrow$ LUMO$+2(\alpha)$	0.23312
HOMO$-2(\alpha) \rightarrow$ LUMO$+3(\alpha)$	-0.22186
HOMO$-1(\alpha) \rightarrow$ LUMO$+1(\alpha)$	0.29428
HOMO$-1(\alpha) \rightarrow$ LUMO$+4(\alpha)$	-0.19547
HOMO$(\alpha) \rightarrow$ LUMO(α)	-0.19493
HOMO$(\alpha) \rightarrow$ LUMO$+5(\alpha)$	0.33454
HOMO$-5(\beta) \rightarrow$ LUMO$+1(\beta)$	0.14682
HOMO$-4(\beta) \rightarrow$ LUMO$+1(\beta)$	-0.22555
HOMO$-4(\beta) \rightarrow$ LUMO$+5(\beta)$	-0.10621
HOMO$-2(\beta) \rightarrow$ LUMO$+2(\beta)$	0.22891
HOMO$-2(\beta) \rightarrow$ LUMO$+3(\beta)$	-0.22087
HOMO$-1(\beta) \rightarrow$ LUMO(β)	0.30519
HOMO$-1(\beta) \rightarrow$ LUMO$+4(\beta)$	-0.20990
HOMO$(\beta) \rightarrow$ LUMO$+1(\beta)$	0.21280
HOMO$(\beta) \rightarrow$ LUMO$+5(\beta)$	0.34087

Table S22. The evaluated nature of transition associated with λ_{max} of ZnPor(ED)$_4$.

ZnPor(ED)$_4$	configuration coefficient
HOMO$-5(\alpha)\rightarrow$ LUMO$+1(\alpha)$	0.14228
HOMO$-4(\alpha)\rightarrow$ LUMO$+1(\alpha)$	-0.22092
HOMO$-4(\alpha)\rightarrow$ LUMO$+5(\alpha)$	-0.10445
HOMO$-2(\alpha)\rightarrow$ LUMO$+2(\alpha)$	-0.22352
HOMO$-2(\alpha)\rightarrow$ LUMO$+3(\alpha)$	0.21577
HOMO$-1(\alpha)\rightarrow$ LUMO(α)	0.29352
HOMO$-1(\alpha)\rightarrow$ LUMO$+4(\alpha)$	0.19030
HOMO$(\alpha)\rightarrow$ LUMO$+1(\alpha)$	0.19983
HOMO$(\alpha)\rightarrow$ LUMO$+5(\alpha)$	0.35232
HOMO$-5(\beta)\rightarrow$ LUMO$+1(\beta)$	0.14228
HOMO$-4(\beta)\rightarrow$ LUMO$+1(\beta)$	-0.22092
HOMO$-4(\beta)\rightarrow$ LUMO$+5(\beta)$	-0.10445
HOMO$-2(\beta)\rightarrow$ LUMO$+2(\beta)$	-0.22352
HOMO$-2(\beta)\rightarrow$ LUMO$+3(\beta)$	0.21577
HOMO$-1(\beta)\rightarrow$ LUMO(β)	0.29352
HOMO$-1(\beta)\rightarrow$ LUMO$+4(\beta)$	0.19030
HOMO$(\beta)\rightarrow$ LUMO$+1(\beta)$	0.19983
HOMO$(\beta)\rightarrow$LUMO$+5(\beta)$	0.35232

Table S23. Calculated lifetime (τ, ns) of MPor using CAM-B3LYP functionals.

	CoPor	NiPor	CuPor	ZnPor
τ (ns)	0.10	0.11	0.12	0.12

Table S24. Calculated relative stabilization energy (kJ.mol^{-1}) of various states of CO_2 adsorption on studied photocatalysts. The states in the parentheses represent the final states of coordination.

Photocatalyst	CA	CB	OA	OB
$CoPor(ED)_4$	2.00 (OA)	0.23 (OB)	1.83 (OA)	0.00 (OB)
$NiPor(ED)_4$	2.43 (CA)	0.31 (CB)	2.19 (OA)	0.00 (OB)
$CuPor(ED)_4$	1.88 (CA)	0.11 (CB)	1.59 (OA)	0.00 (OB)
$ZnPor(ED)_4$	2.12 (OA)	0.89 (OB)	1.54 (OA)	0.00 (OB)

Table S25. Covalent atomic radii (d_C, Å) of Co, Ni, Cu , Zn, and O atom.[8]

Atom type	d_C (Å)
Co	1.26
Ni	1.24
Cu	1.32
Zn	1.22
O	0.66

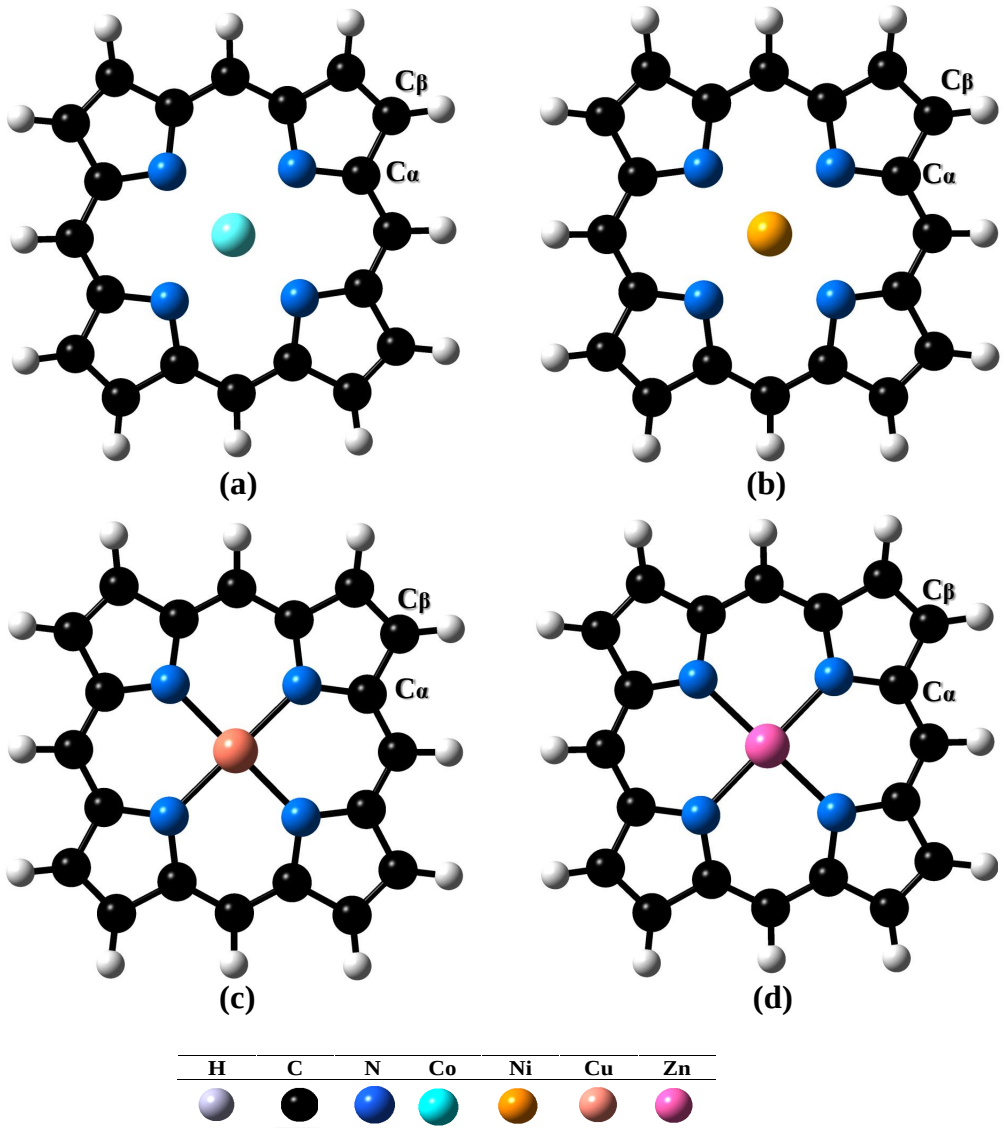

Figure S1. The relaxed geometric structures of four catalysts active sites (a) CoPor (b) NiPor (c) CuPor, and (d) ZnPor are used in this study.

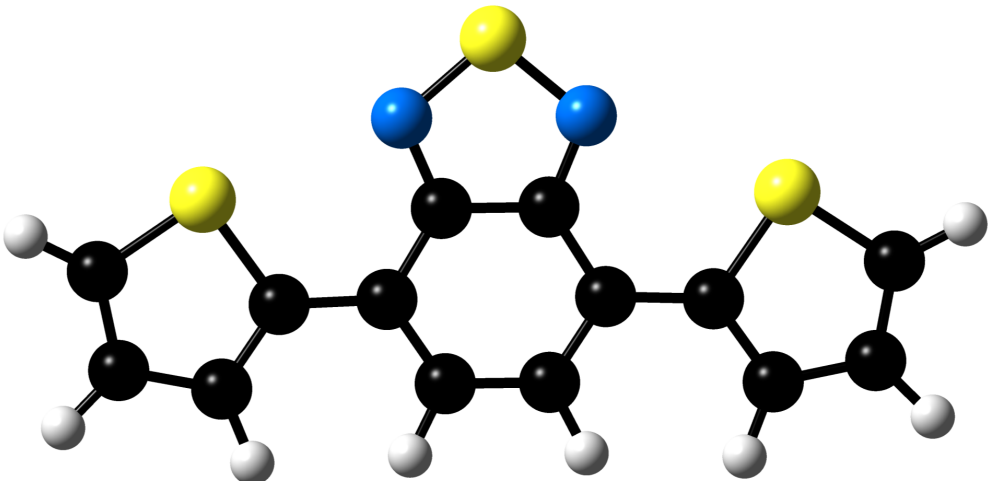

Figure S2. The relaxed geometric structures of the ED is used in this study.

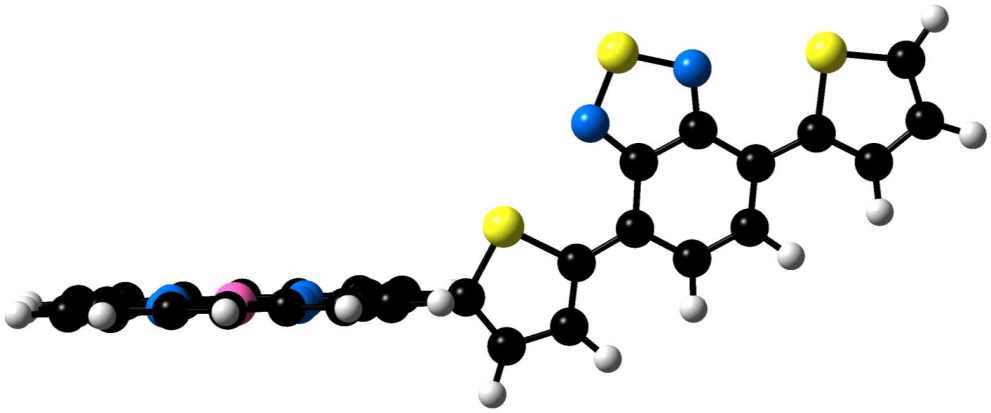

Figure S3. The relaxed geometric structures of the ZnPor−ED. In this structure the catalyst active site and ED are connected directly.

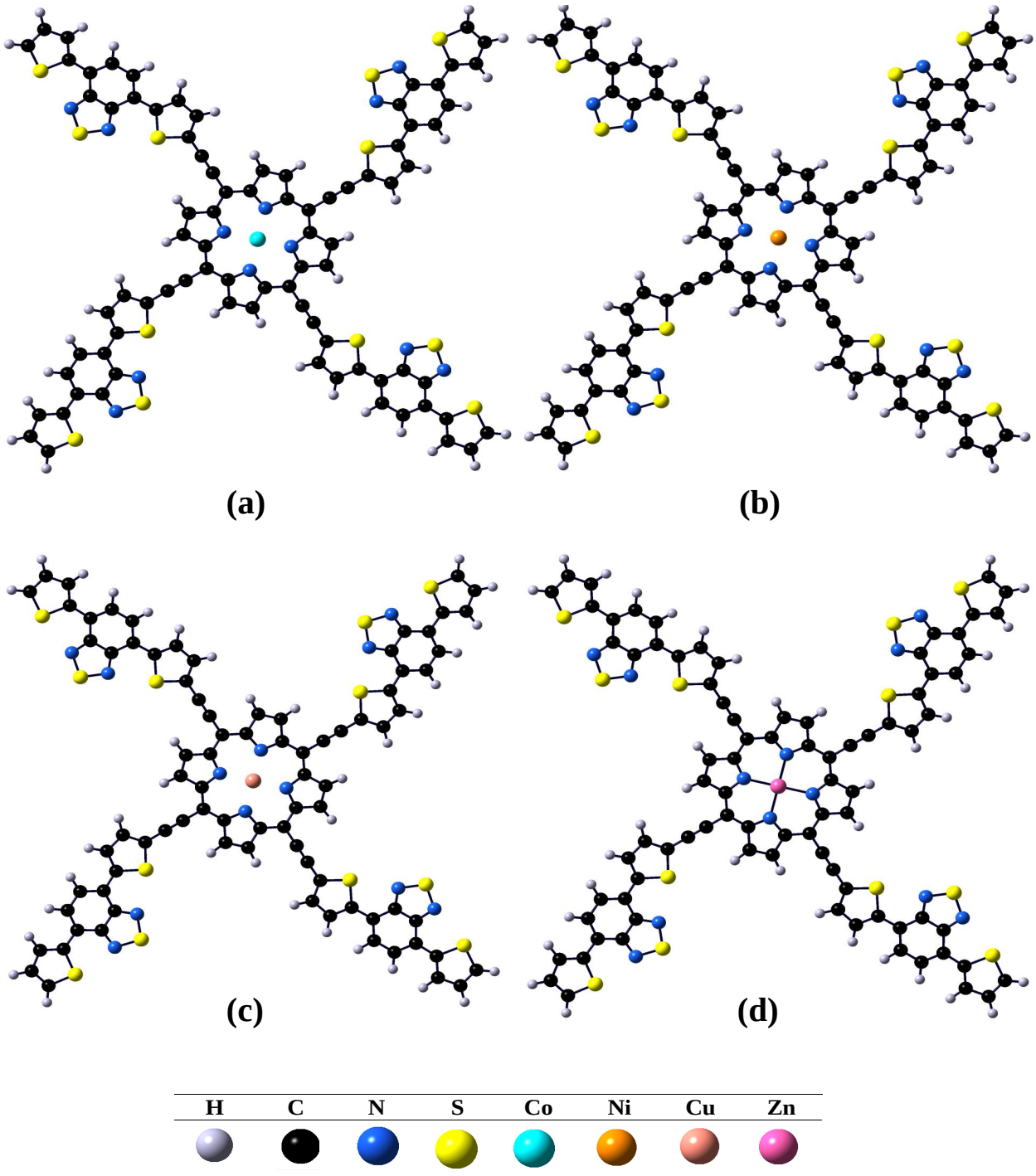

Figure S4. The relaxed geometric structures of (a) $CoPor(ED)_4$ (b) $NiPor(ED)_4$ (c) $CuPor(ED)_4$, and (d) $ZnPor(ED)_4$ catalysts are used in this study.

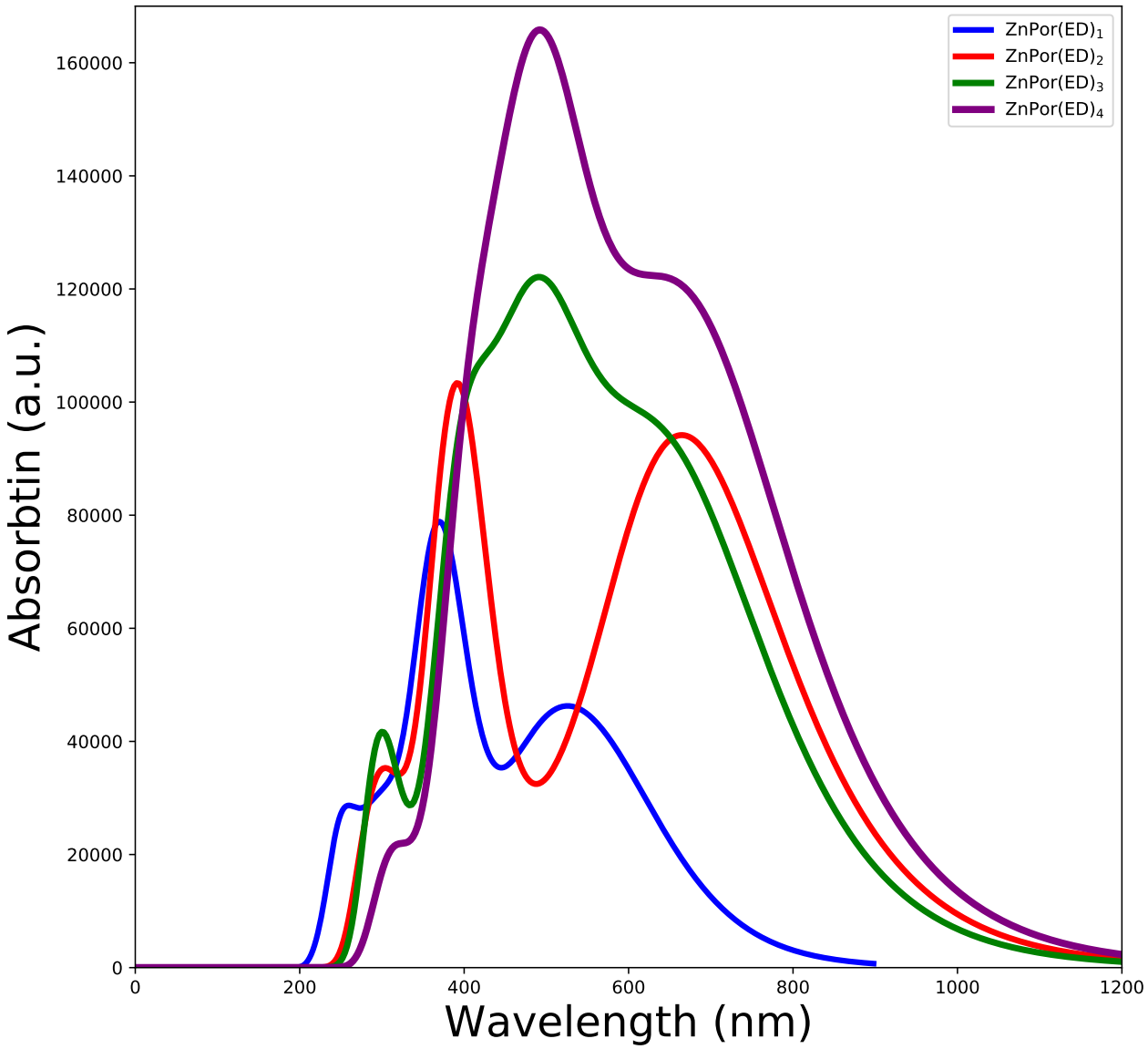

Figure S5. UV−Vis spectra of the ZnPor(ED)$_n$ with $n = 1 - 4$.

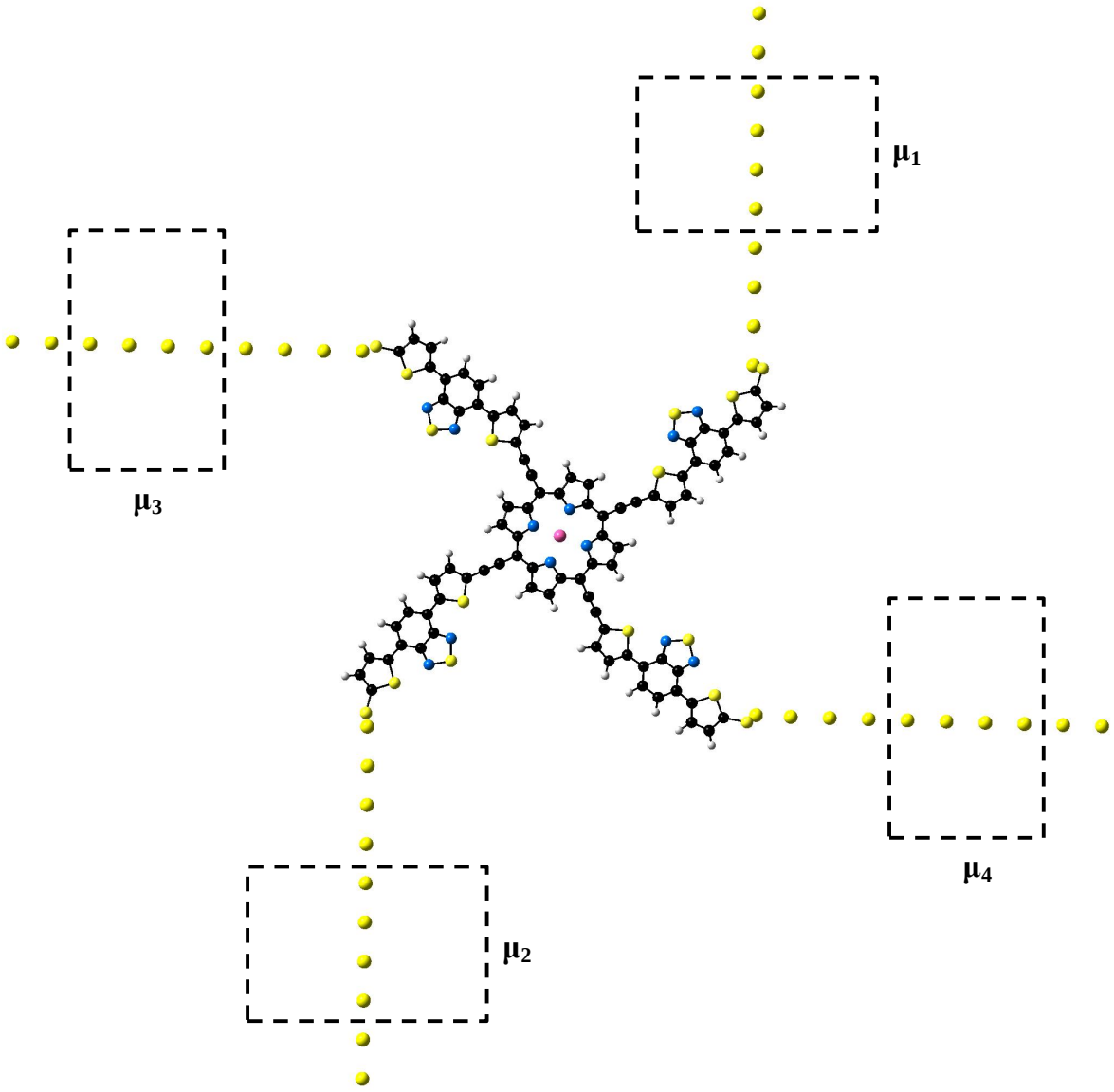

Figure S6. Structure of four-terminal ZnPor(ED)$_4$ devices before CO_2 adsorption. The boxed regions indicated four semi-infinite GNWs electrodes. The μ_1, μ_2, μ_3 and μ_4 represent the electrode chemical potential. A buffer regions is located behind each electrode act as additional screening region when calculating the initial NEGF guess.

LUMO+5(α)

LUMO+5(β)

LUMO+4(α)

LUMO+4(β)

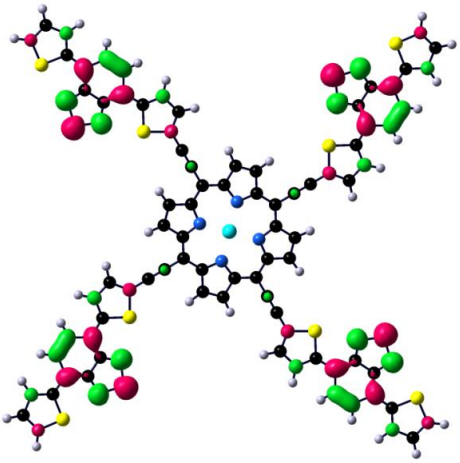

LUMO+3(α)

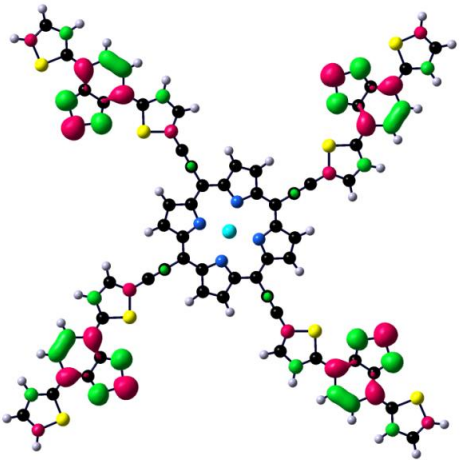

LUMO+3(β)

Figure S7. Frontier and subfrontier MOs of the CoPor(ED)$_4$ photocatalyst.

LUMO+2(α)

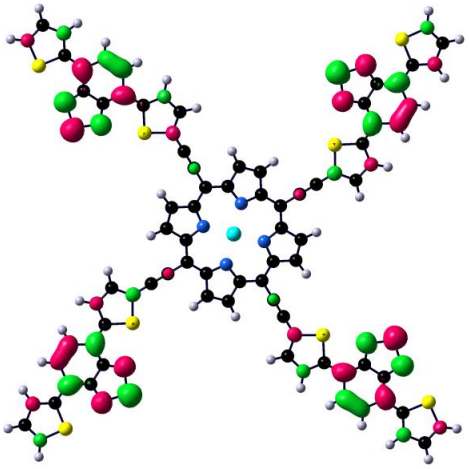

LUMO+2(β)

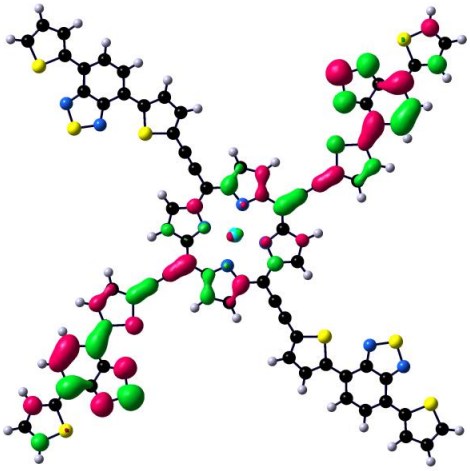

LUMO+1(α)

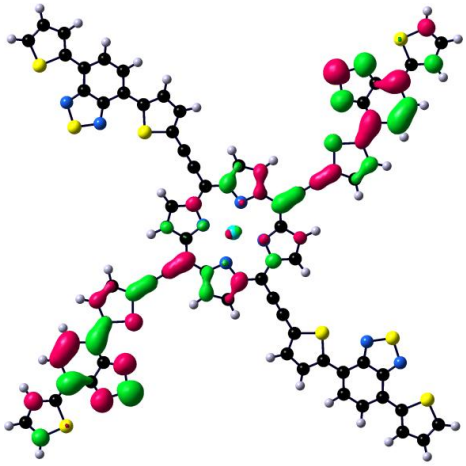

LUMO+1(β)

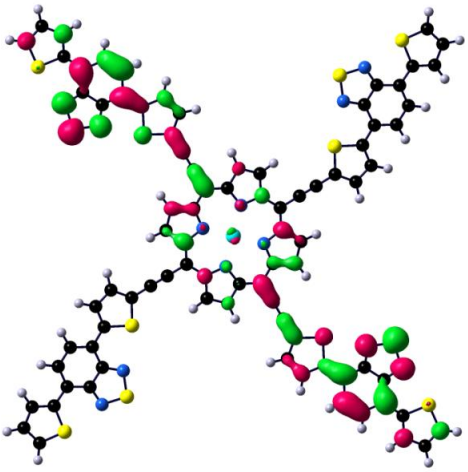

LUMO(α)

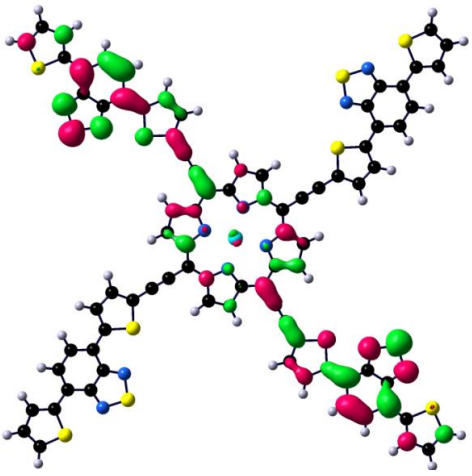

LUMO(β)

Frontier and subfrontier MOs of the CoPor(ED)$_4$ photocatalyst.

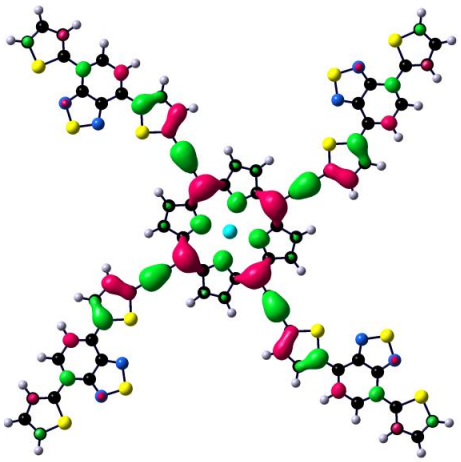

SOMO(α) [HOMO(α)]

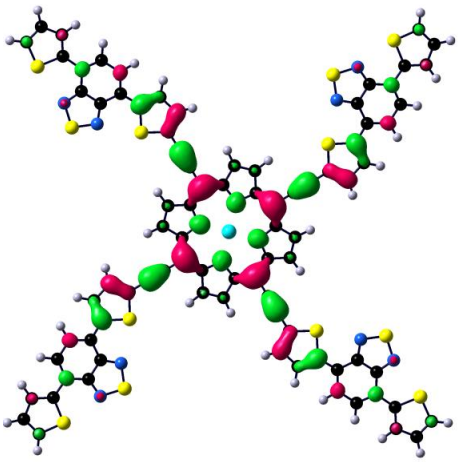

SOMO(β) [HOMO(β)]

SOMO–1(α) [HOMO-1(α)]

SOMO–1(β) [HOMO-1(β)]

SOMO–2(α) [HOMO-2(α)]

SOMO–2(β) [HOMO-2(β)]

Frontier and subfrontier MOs of the CoPor(ED)$_4$ photocatalyst.

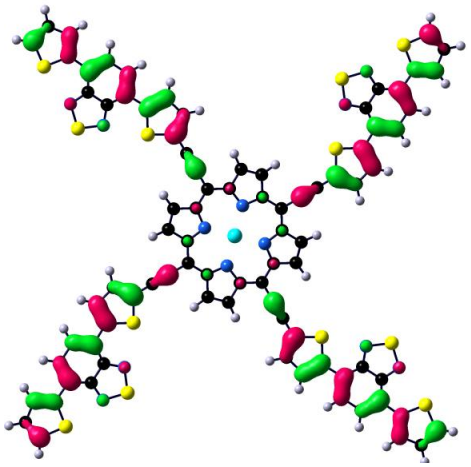

SOMO–3(α) [HOMO-3(α)]

SOMO–3(β) [HOMO-3(β)]

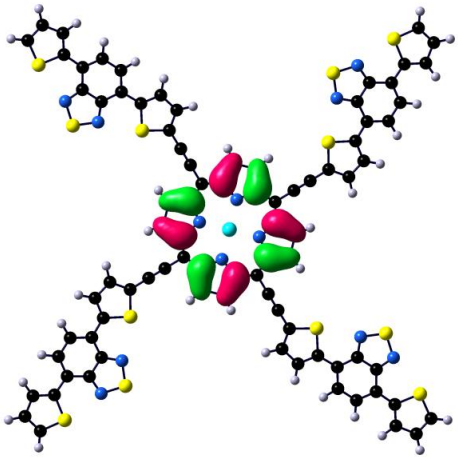

SOMO–4(α) [HOMO-4(α)]

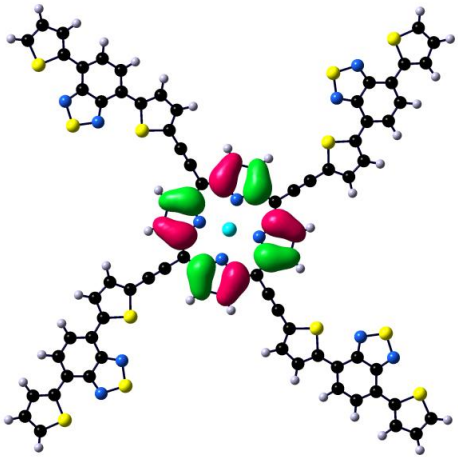

SOMO–4(β) [HOMO-4(β)]

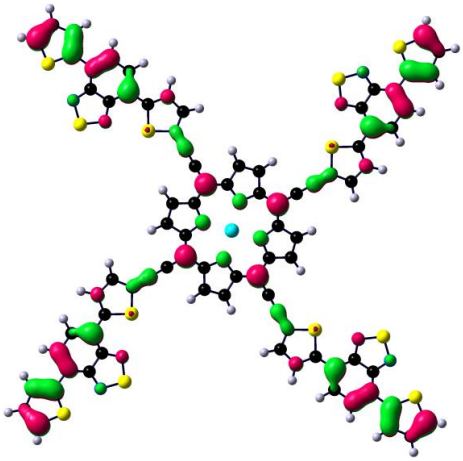

SOMO–5(α) [HOMO-5(α)]

SOMO–5(β) [HOMO-5(β)]

Frontier and subfrontier MOs of the CoPor(ED)$_4$ photocatalyst.

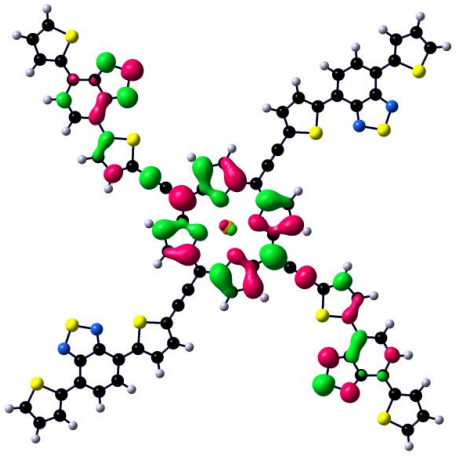

LUMO+5(α)

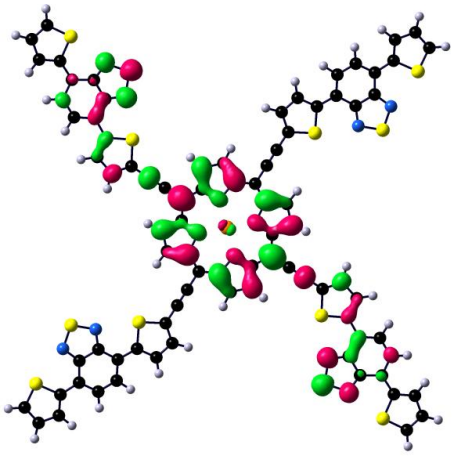

LUMO+5(β)

LUMO+4(α)

LUMO+4(β)

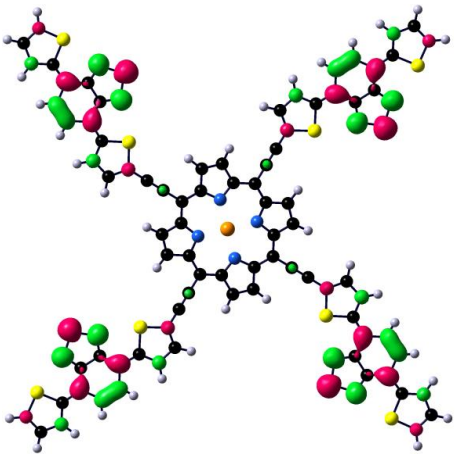

LUMO+3(α)

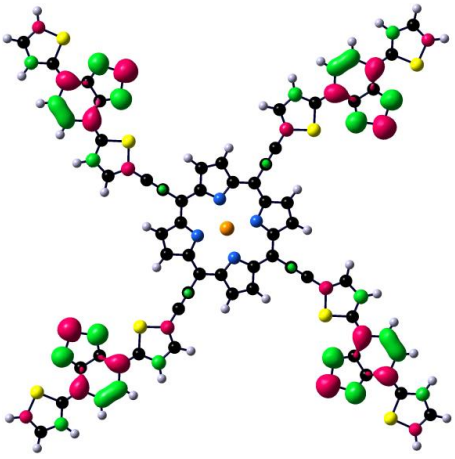

LUMO+3(β)

Figure S8. Frontier and subfrontier MOs of the NiPor(ED)$_4$ photocatalyst.

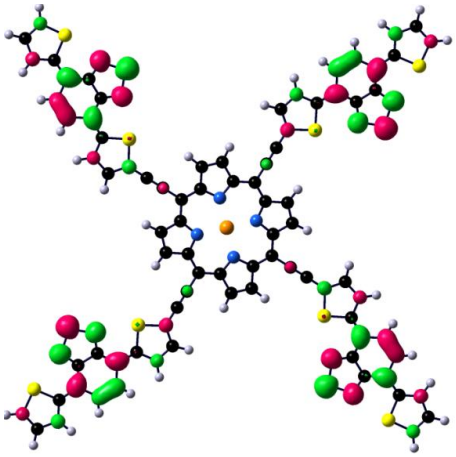

LUMO+2(α)

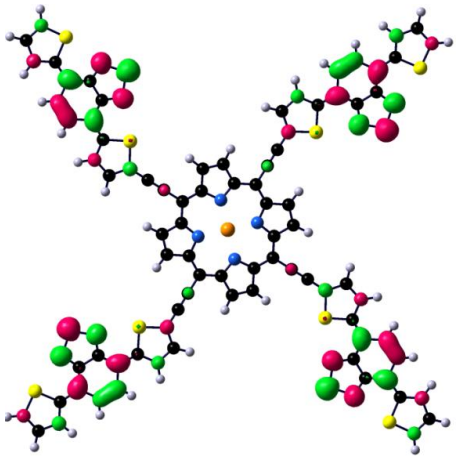

LUMO+2(β)

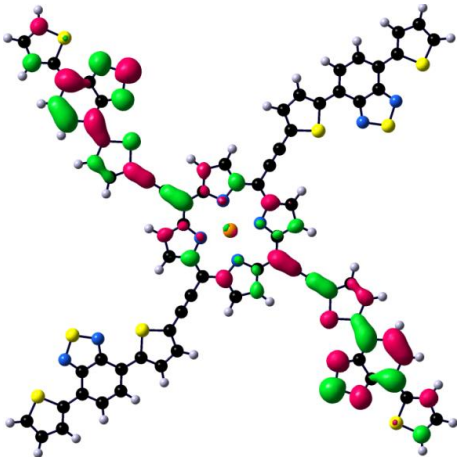

LUMO+1(α)

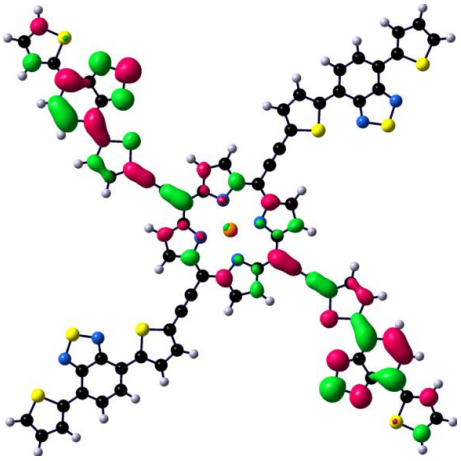

LUMO+1(β)

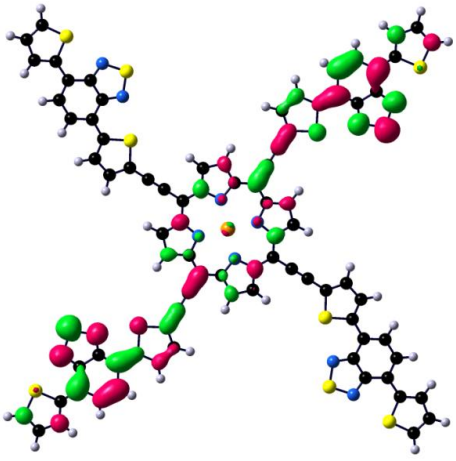

LUMO(α)

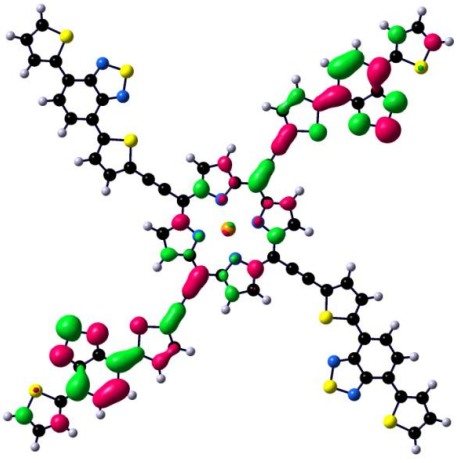

LUMO(β)

Frontier and subfrontier MOs of the NiPor$(ED)_4$ photocatalyst.

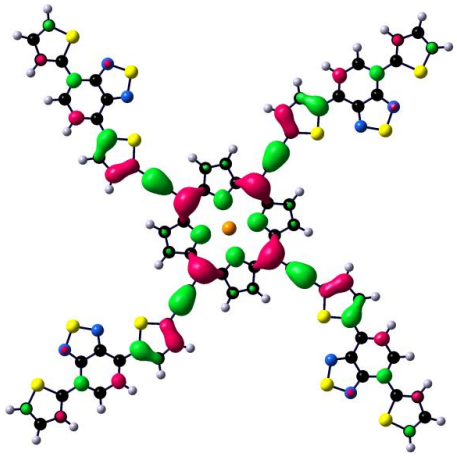

SOMO(α) [HOMO(α)]

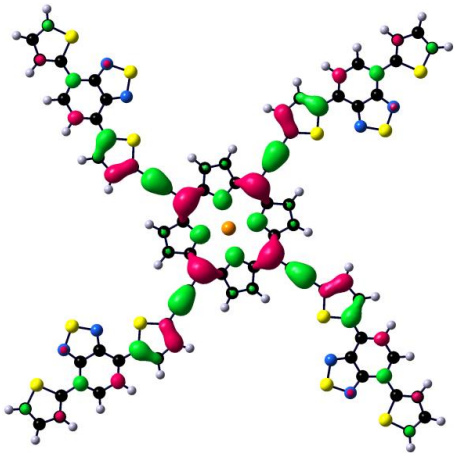

SOMO(β) [HOMO(β)]

SOMO–1(α) [HOMO-1(α)]

SOMO–1(β) [HOMO-1(β)]

SOMO–2(α) [HOMO-2(α)]

SOMO–2(β) [HOMO-2(β)]

Frontier and subfrontier MOs of the NiPor(ED)$_4$ photocatalyst.

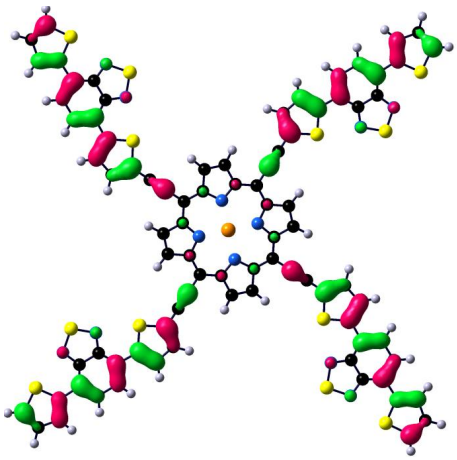

SOMO–3(α) [HOMO-3(α)]

SOMO–3(β) [HOMO-3(β)]

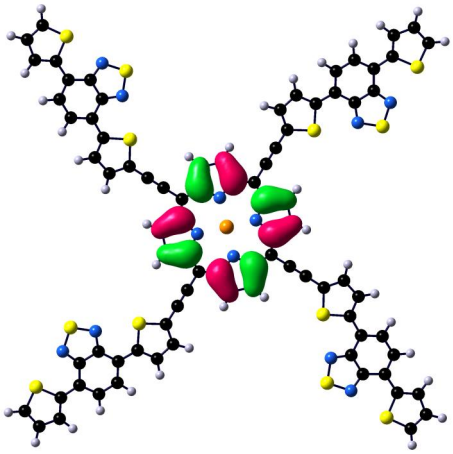

SOMO–4(α) [HOMO-4(α)]

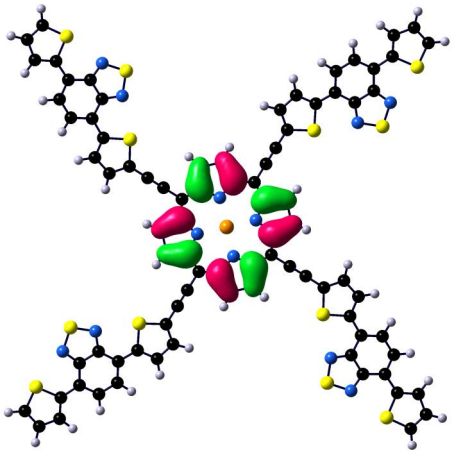

SOMO–4(β) [HOMO-4(β)]

SOMO–5(α) [HOMO-5(α)]

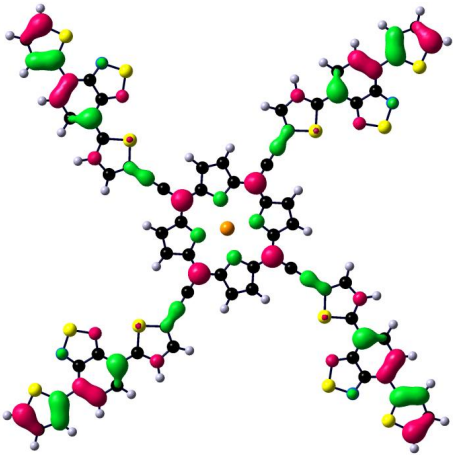

SOMO–5(β) [HOMO-5(β)]

Frontier and subfrontier MOs of the NiPor$(ED)_4$ photocatalyst.

LUMO+5(α)

LUMO+5(β)

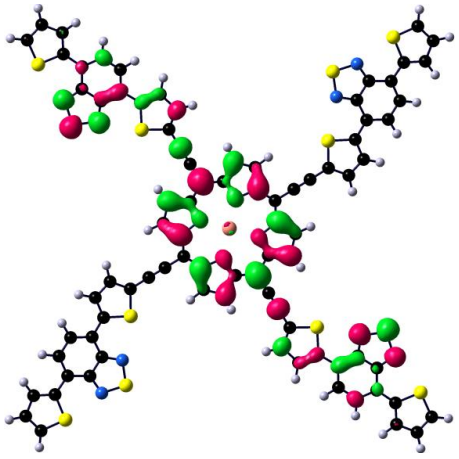

LUMO+4(α)

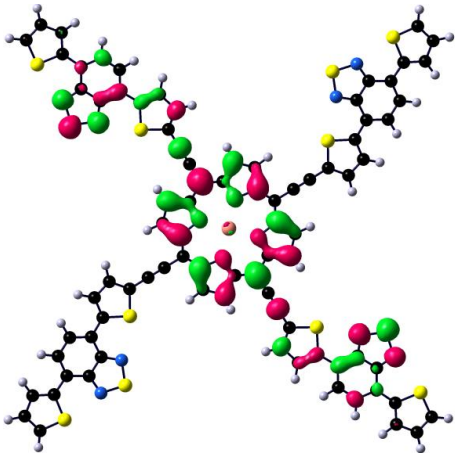

LUMO+4(β)

LUMO+3(α)

LUMO+3(β)

Figure S9. Frontier and subfrontier MOs of the CuPor(ED)$_4$ photocatalyst.

LUMO+2(α)

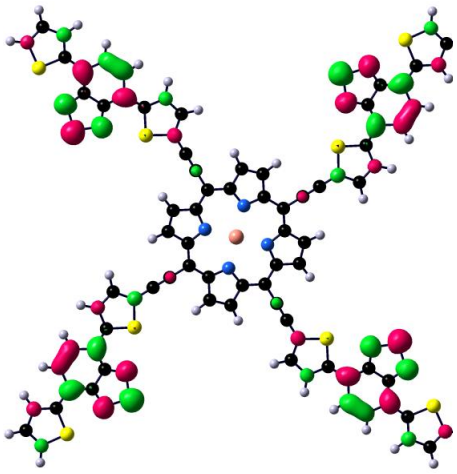

LUMO+2(β)

LUMO+1(α)

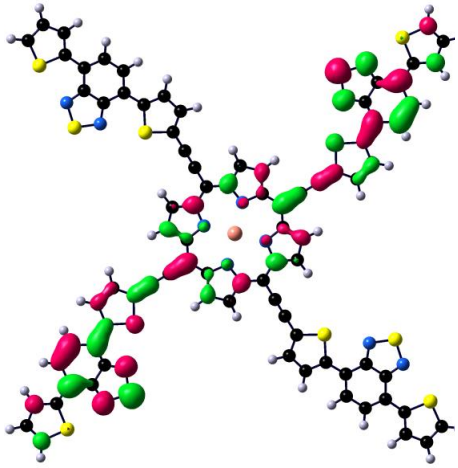

LUMO+1(β)

LUMO(α)

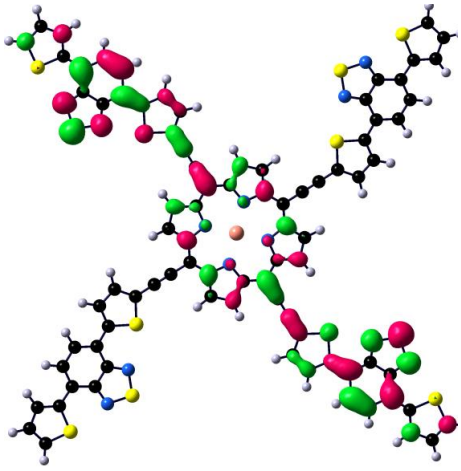

LUMO(β)

Frontier and subfrontier MOs of the CuPor(ED)$_4$ photocatalyst.

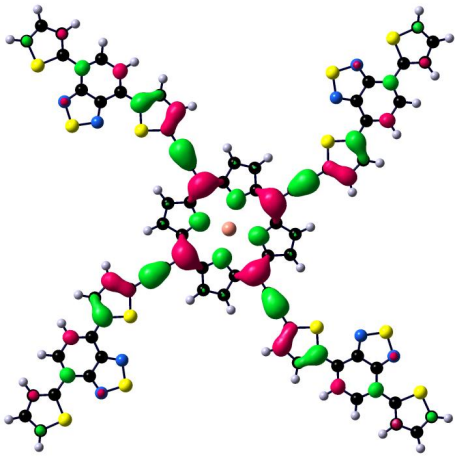

SOMO(α) [HOMO(α)]

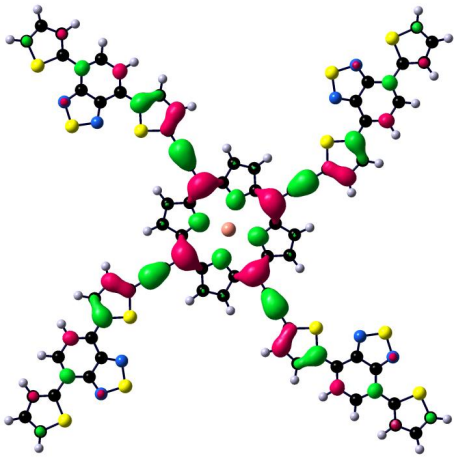

SOMO(β) [HOMO(β)]

SOMO–1(α) [HOMO-1(α)]

SOMO–1(β) [HOMO-1(β)]

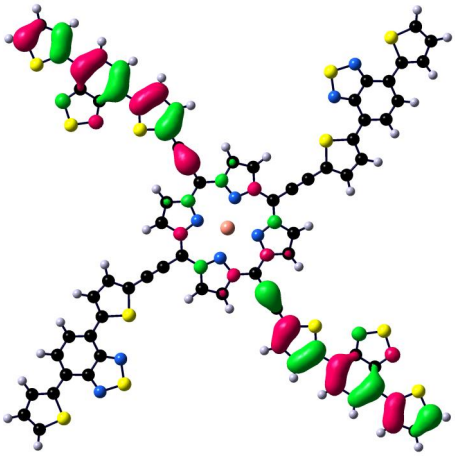

SOMO–2(α) [HOMO-2(α)]

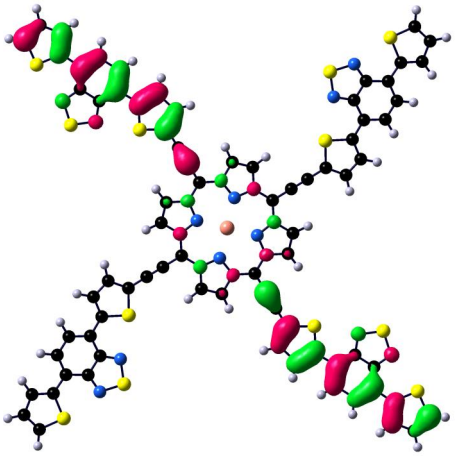

SOMO–2(β) [HOMO-2(β)]

Frontier and subfrontier MOs of the CuPor(ED)$_4$ photocatalyst.

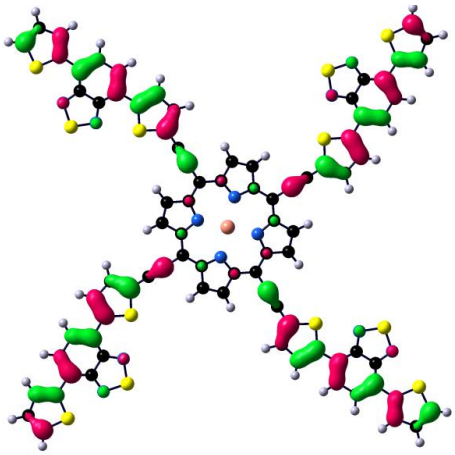

SOMO–3(α) [HOMO-3(α)]

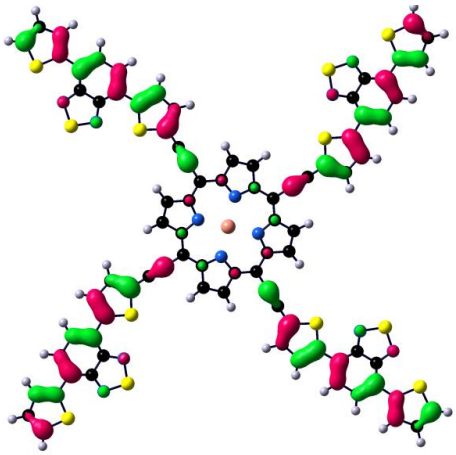

SOMO–3(β) [HOMO-3(β)]

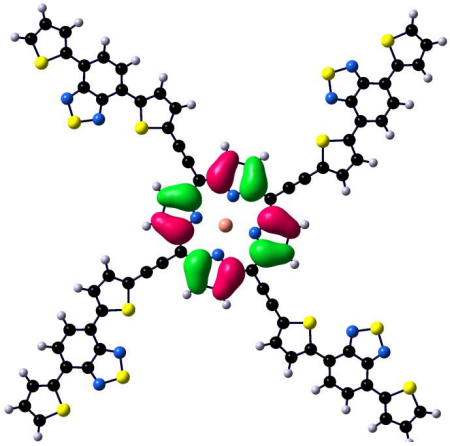

SOMO–4(α) [HOMO-4(α)]

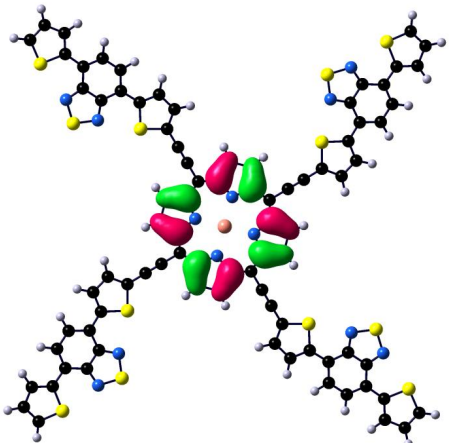

SOMO–4(β) [HOMO-4(β)]

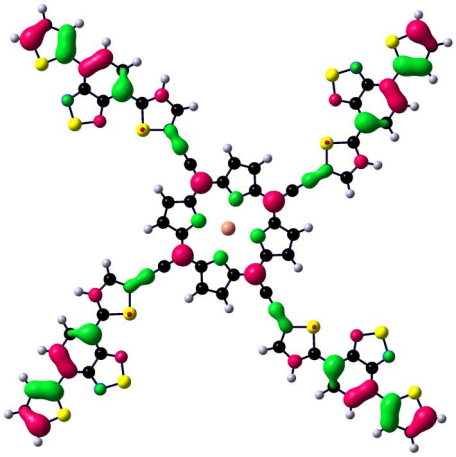

SOMO–5(α) [HOMO-5(α)]

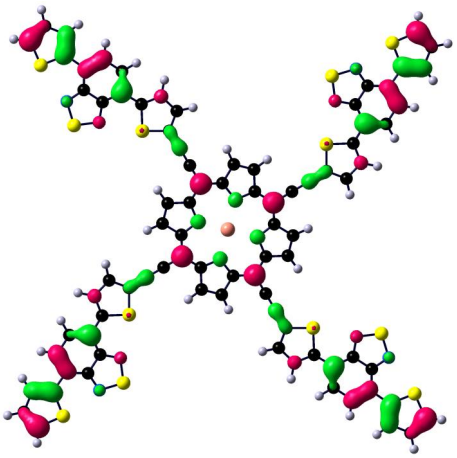

SOMO–5(β) [HOMO-5(β)]

Frontier and subfrontier MOs of the CuPor(ED)$_4$ photocatalyst.

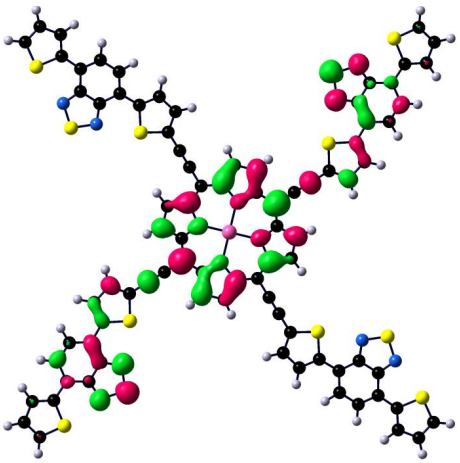

LUMO+5(α)

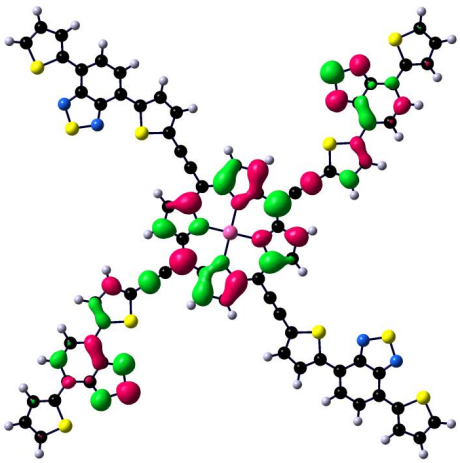

LUMO+5(β)

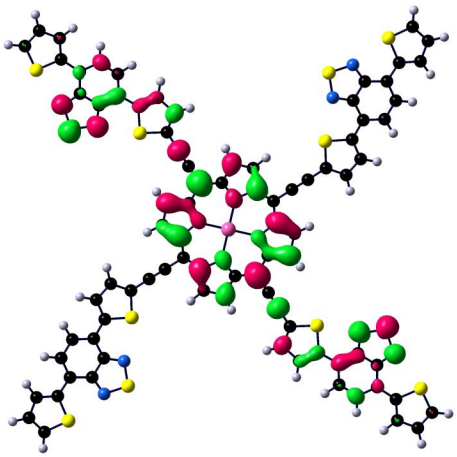

LUMO+4(α)

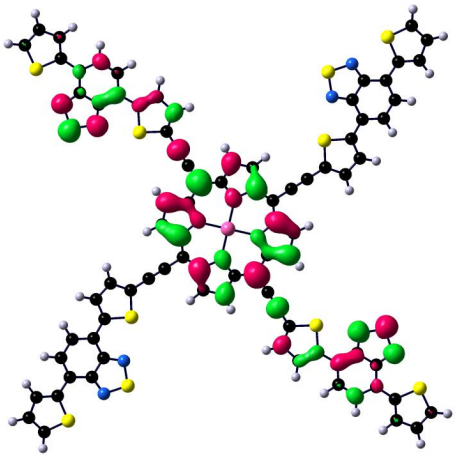

LUMO+4(β)

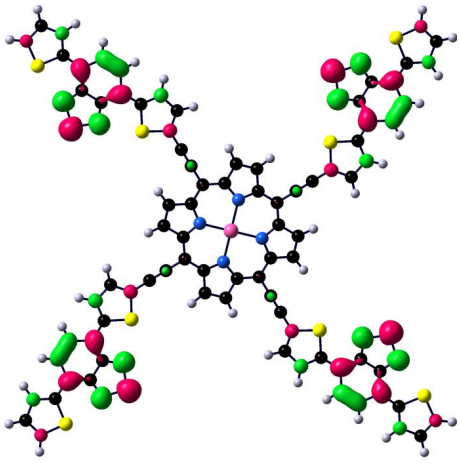

LUMO+3(α)

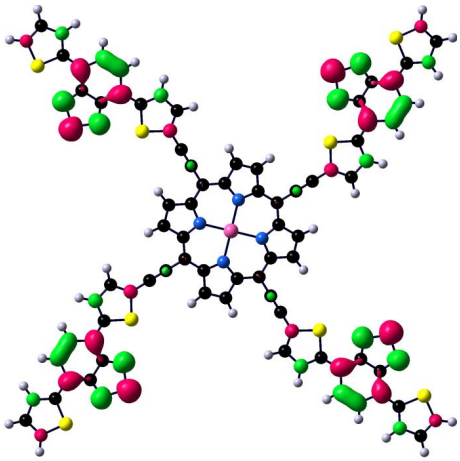

LUMO+3(β)

Figure S10. Frontier and subfrontier MOs of the ZnPor(ED)$_4$ photocatalyst.

LUMO+2(α)

LUMO+2(β)

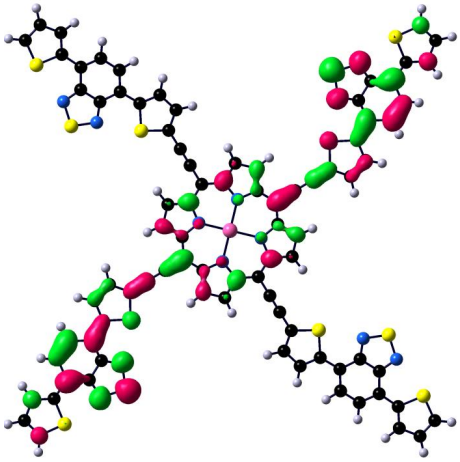

LUMO+1(α)

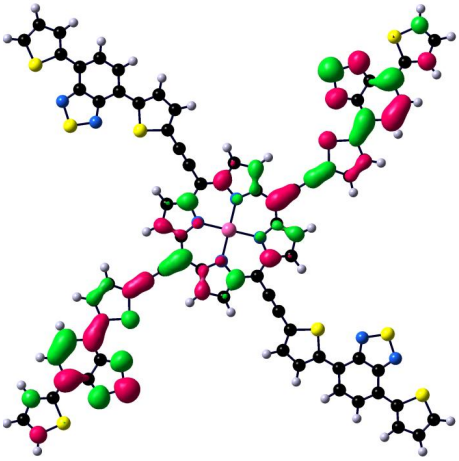

LUMO+1(β)

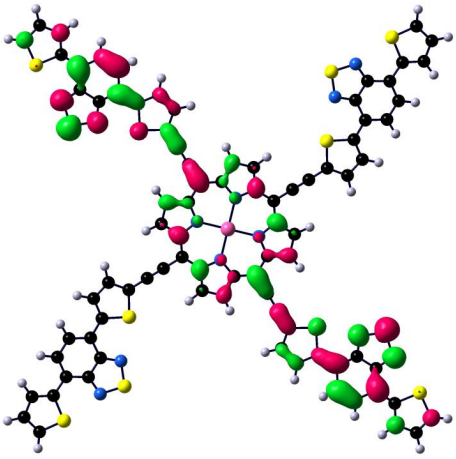

LUMO(α)

LUMO(β)

Frontier and subfrontier MOs of the ZnPor(ED)$_4$ photocatalyst.

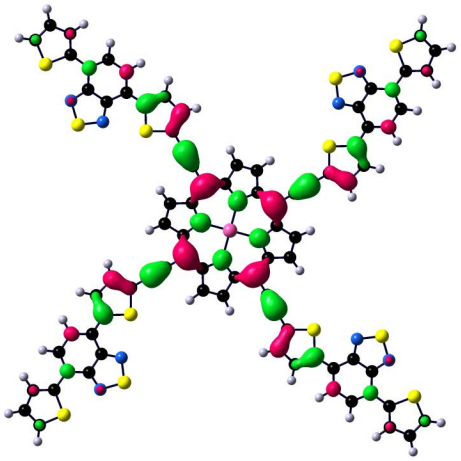

SOMO(α) [HOMO(α)]

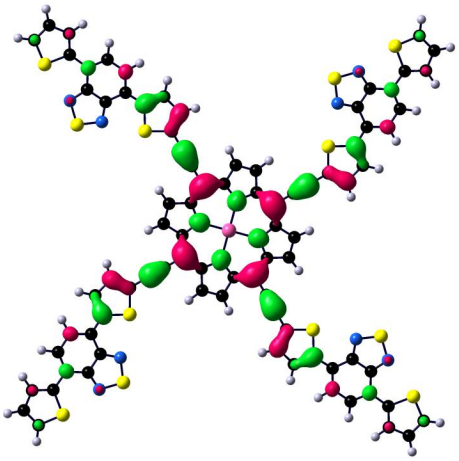

SOMO(β) [HOMO(β)]

SOMO–1(α) [HOMO-1(α)]

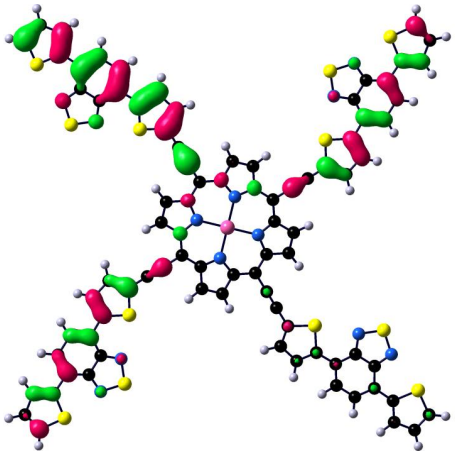

SOMO–1(β) [HOMO-1(β)]

SOMO–2(α) [HOMO-2(α)]

SOMO–2(β) [HOMO-2(β)]

Frontier and subfrontier MOs of the ZnPor(ED)$_4$ photocatalyst.

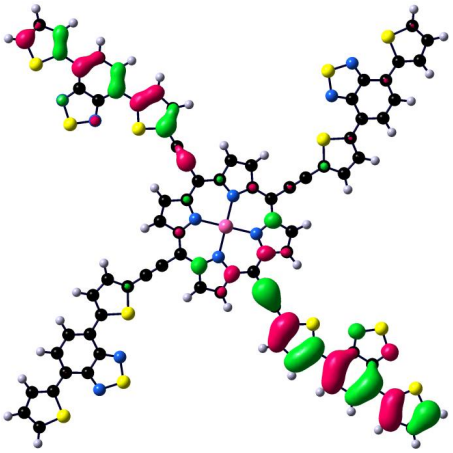

SOMO–3(α) [HOMO-3(α)]

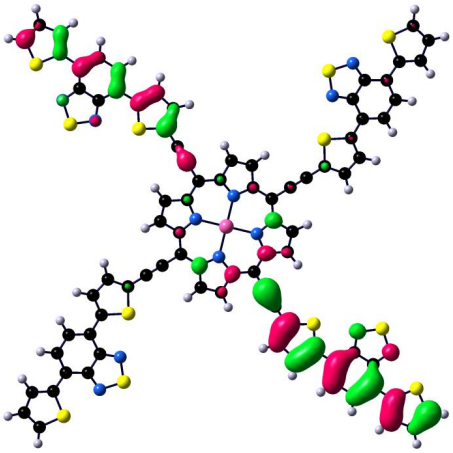

SOMO–3(β) [HOMO-3(β)]

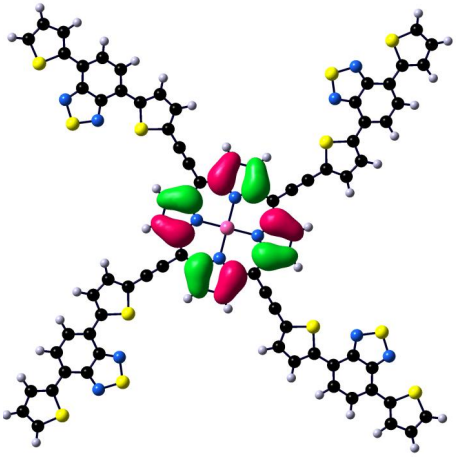

SOMO–4(α) [HOMO-4(α)]

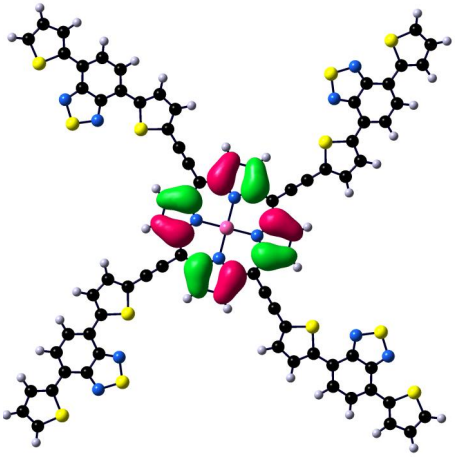

SOMO–4(β) [HOMO-4(β)]

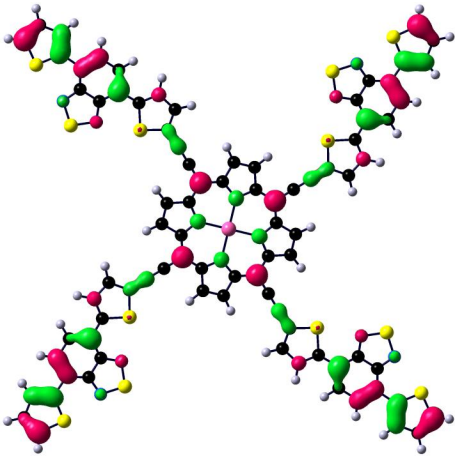

SOMO–5(α) [HOMO-5(α)]

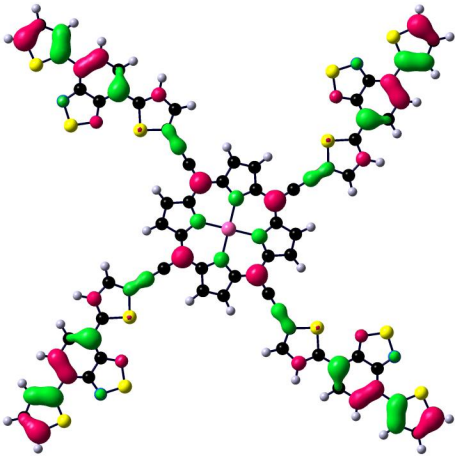

SOMO–5(β) [HOMO-5(β)]

Frontier and subfrontier MOs of the ZnPor$(ED)_4$ photocatalyst.

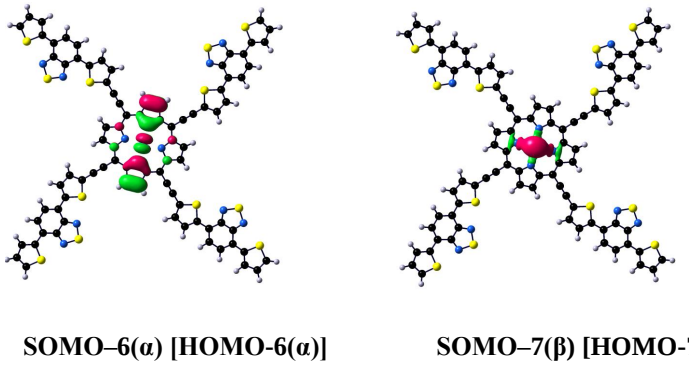

Figure S11. The HOMO energy level of studied photocatalysts with metal contribution (a) $CoPor(ED)_4$ (b) $NiPor(ED)_4$ (c) $CuPor(ED)_4$ and (d) $ZnPor(ED)_4$

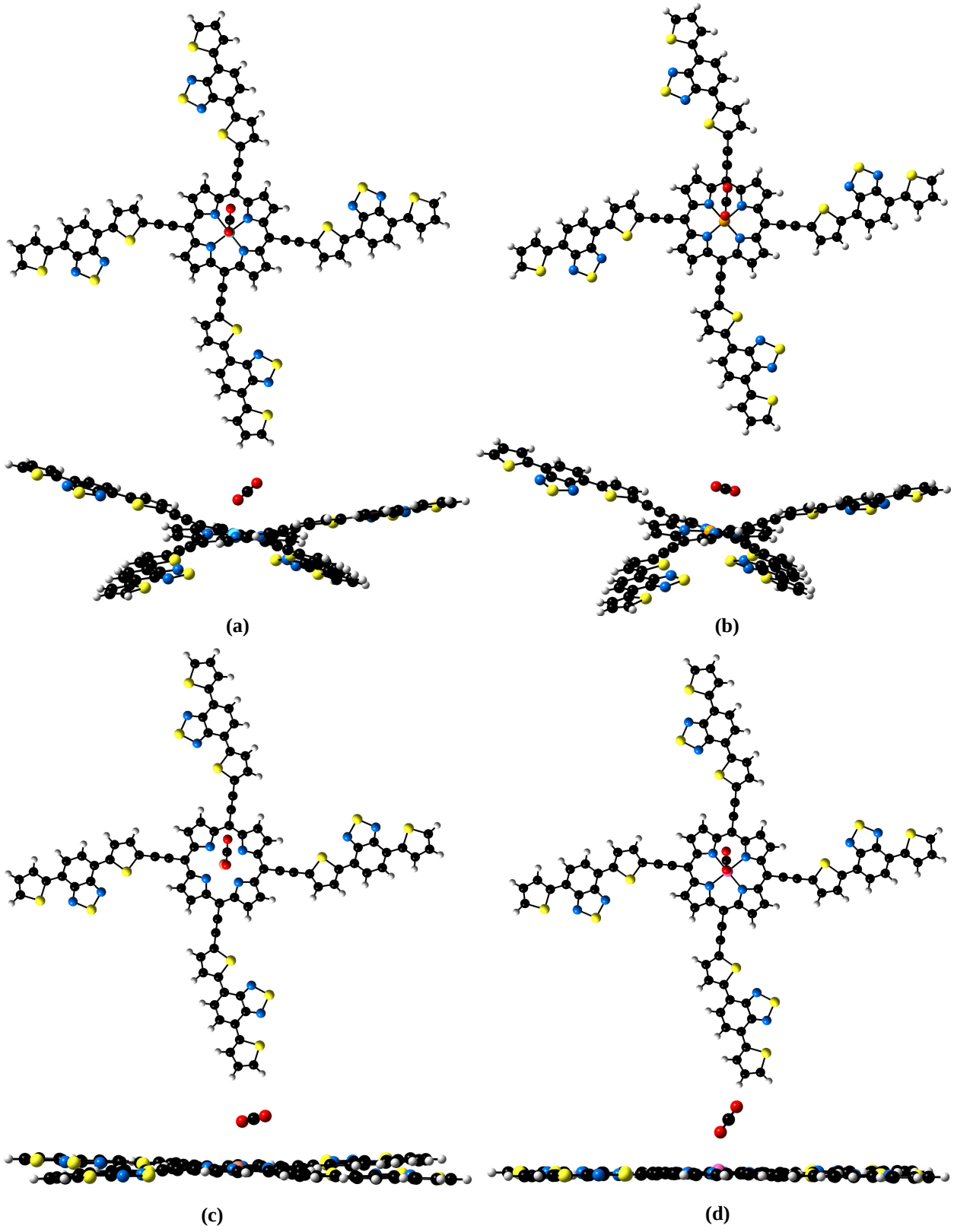

Figure S12. The relaxed geometric structure of the most stable states in CO_2 adsorption (a) $CoPor(ED)_4$, (b) $NiPor(ED)_4$, (c) $CuPor(ED)_4$, and (d) $ZnPor(ED)_4$ nanoreactors. The top and side views of each photocatalyst are shown in corresponding part.

References

1 W. R. Scheidt and I. Turowska-Tyrk, Inorg. Chem., 1994, 33, 1314−1318.

2 W. Jentzen, I. Turowska-Tyrk, W. R. Scheidt and J. A. Shelnutt, Inorg. Chem., 1996, 35, 3559−3567.

3 E. B. Fleischer, C. K. Miller and L. E. Webb, J. Am. Chem. Soc., 1964, 86, 2342−2347.

4 A. Ozarowski, H. M. Lee and A. L. Balch, J. Am. Chem. Soc., 2003, 125, 12606−12614.

5 D. R. Roy, E. V. Shah and S. M. Roy, Spectrochim. Acta A Mol. Biomol. Spectrosc., 2018, 190, 121−128.

6 M. B. M. Krishna, N. Venkatramaiah and D. N. Rao, J. Opt., 2013, 16, 015205.

7 P. Ledwon, N. Thomson, E. Angioni, N. J. Findlay, P. J. Skabara and W. Domagala, RSC Adv., 2015, 5, 77303−77315.

8 B. Cordero, V. Gómez, A. E. Platero-Prats, M. Revés, J. Echeverría, E. Cremades, F. Barragán and S. Alvarez, Dalton Trans., 2008, 21, 2832−2838.